CHAPTER 5

Molecular Engineering of Cellular Environments: Cell Adhesion to Nano-Digital Surfaces

Joachim P. Spatz[*] and Benjamin Geiger[†]

[*]Department of New Materials and Biosystems
Max Planck Institute for Metals Research
Stuttgart, Germany; and Department of Biophysical Chemistry
University of Heidelberg, Heidelberg, Germany

[†]Department of Molecular Cell Biology
Weizmann Institute of Science
Rehovot 76100, Israel

Abstract

Engineering of the cellular microenvironment has become a valuable means to guide cellular activities such as spreading, motility, differentiation, proliferation, or apoptosis. This chapter summarizes recent approaches to surface patterning

METHODS IN CELL BIOLOGY, VOL. 83

0091-679X/07 $35.00
DOI: 10.1016/S0091-679X(07)83005-6

such as topography and chemical patterning from the micrometer to the nanometer scale, and illustrates their application to cellular studies. Particular attention is devoted to nanolithography with self-assembled diblock copolymer micelles that are biofunctionalized with peptide ligands—a method that offers unsurpassed spatial resolution for the positioning of signaling molecules over extended surface areas. Such interfaces are defined here as "nano-digital surfaces," since they enable the counting of individual signaling complexes separated by a biologically inert background. The approach enables the testing of cellular responses to individual signaling molecules as well as their *spatial* ordering. Detailed consideration is also given to the fact that protein clusters such as those found at focal adhesion sites represent, to a large extent, hierarchically organized cooperativity among various proteins.

I. Introduction: Sensing Cellular Environments

Cell adhesion to the extracellular matrix (ECM) and to neighboring cells is a complex, tightly regulated process that plays a crucial role in fundamental cellular functions, including cell migration, proliferation, differentiation, and apoptosis (Blau and Baltimore, 1991; Ruoslahti and Obrink, 1996). By interacting directly with such external surfaces, cells gather information about the chemical and physical nature of the ECM, integrate and interpret it, and then generate an appropriate physiological response. The mechanism underlying the capacity of cells to perform such "intelligence missions" of data acquisition and processing is still poorly understood at the molecular level, although it is likely that the cell's adhesive machinery as well as associated cytoskeletal and signaling networks play a major role (Vogel and Sheetz, 2006).

What molecular features of the environment can cells sense? In principle, cells monitor differences between soluble and immobilized signaling molecules. Soluble factors are capable of activating specific signaling networks. Spatial resolution of different chemical concentrations is given by chemoattractant gradients. However, their spatial resolution is rather low, that is, in the range of a few micrometers when applying microfluidic devices (Lin and Butcher, 2006).

Examination of the structure of the ECM provides strong evidence that the presentation of signaling molecules to cells in a defined microscopic as well as nanoscopic geometry affects cell response with great consequences, provided that cells are in direct contact with the ECM. Figure 1A presents a transmission electron microscopy image of an epidermal cell, that is fibroblast, which is extensively embedded in a network of collagen fibers organized into bundles that run approximately at right angles to each other (Alberts *et al.*, 2001, p. 1098, Figs. 19–44; Ploetz *et al.*, 1991). Figure 1B presents a scanning force microscopy (SFM) image of a collagen fiber bundle as visualized in Fig. 1A. Since SFM provides nanoscopic resolution based on sensing topographic or mechanical differences on surfaces, fibers of collagen are displayed with a periodic corrugation of

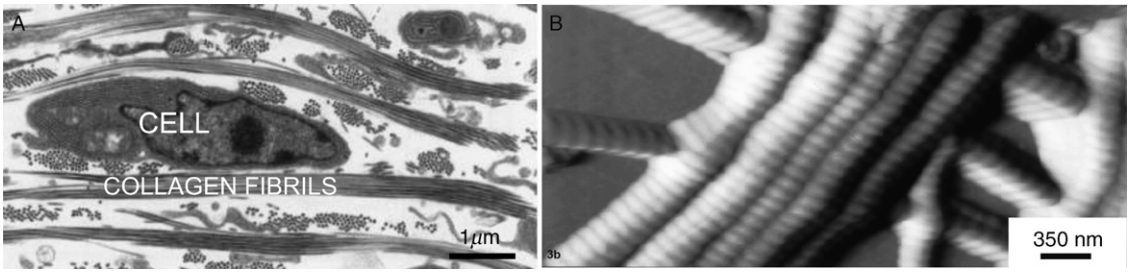

Fig. 1 (A) Fibroblast surrounded by collagen fibrils in the connective tissue (Alberts *et al.*, 2001 and modified from Ploetz *et al.*, 1991). (B) SFM of scleral collagen fibrils displaying ~67-nm periodicity of collagen fibrils (from Meller *et al.*, 1997).

~67 nm (Meller *et al.*, 1997). Such a periodicity is typically observed for collagen type one as also observed by scanning electron microscopy (SEM) or x-ray scattering (Fratzl *et al.*, 1998; Jiang *et al.*, 2004). From such structural observations, it becomes evident that the ECM presents a hierarchy of different length scales and viscoelasticities to cell surfaces. A key question in cell biology is how spatial positioning of signaling cues as well as variations in local rigidity of the ECM at different length scales affects cell responses.

Tissue cells respond to the presented environment with adhesion if appropriate conditions are given. Cells are able to sense differences in physical conditions such as different chemical or mechanical properties. Cells may distinguish between surfaces of different chemical properties due to the differential activation of distinct surface receptors on interactions with the particular repertoire of ligands on these surfaces. Such diverse interactions may then trigger a wide variety of cellular responses.

Rigidity of a cell's environment was identified as a marker that provides essential information to cells. Cells sense differences in rigidity of the adhesive environment which in turn strongly affects the fate of cells (Discher *et al.*, 2005; Georges and Janmey, 2005). A variety of receptors are involved in the cell's local interactions with the external surface (Fig. 2A). The best-characterized systems consist of micrometer-sized, multiprotein complexes called focal adhesions (FA) (Fig. 2A) and related structures, including focal complexes, which are small nascent adhesions formed under the leading lamellae (Ballestrem *et al.*, 2001; Zamir and Geiger, 2001a), and fibrillar adhesions formed with fibronectin networks and consisting of integrin receptors and a wide variety of cytoskeletal and signaling proteins (Fig. 1A) (Critchley, 2000; Geiger *et al.*, 2001; Giancotti and Ruoslahti, 1999; Hynes, 1987; Levenberg *et al.*, 1998; Miyamoto *et al.*, 1995; Zamir and Geiger, 2001a,b; for an overview, see Fig. 2B). The assembly of these molecules at nascent adhesion sites triggers the reorganization of the actin cytoskeleton, which in turn generates local forces by activating the motor activity of myosins (Balaban *et al.*, 2001).

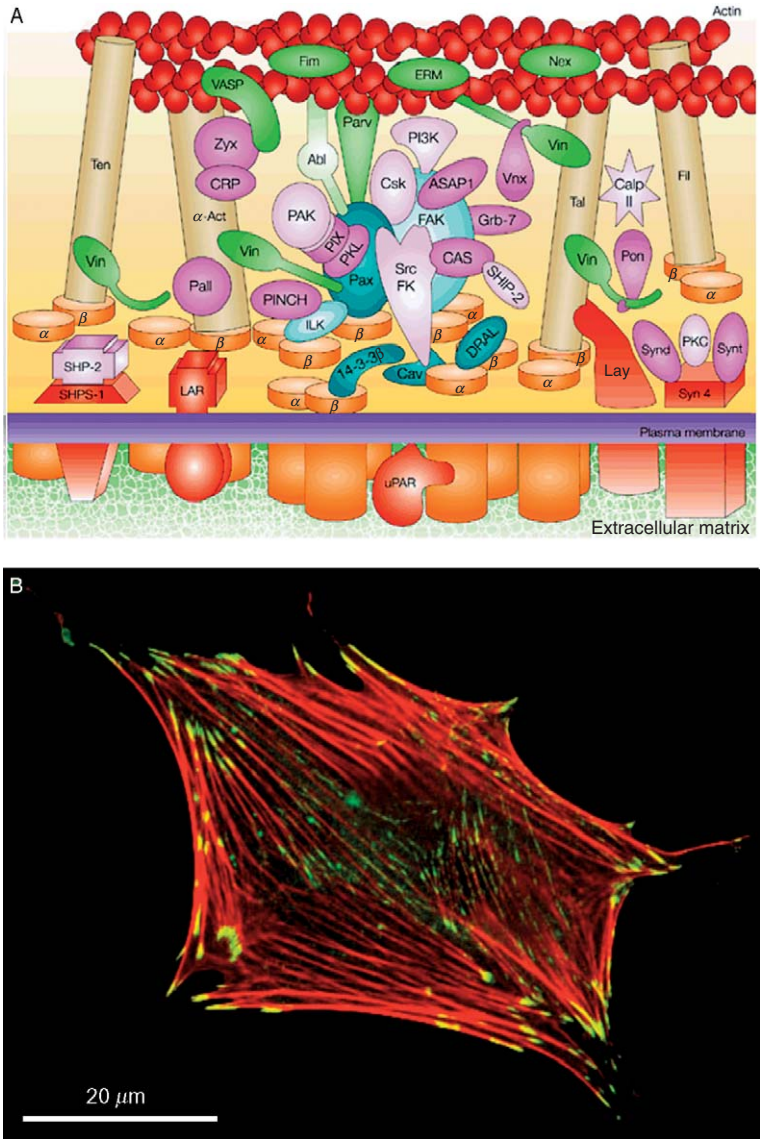

Fig. 2 (A) Schematic presentation (updated, 2001) of the complexity of the main molecular domains of cell–matrix adhesions (Geiger *et al*., 2001; Zamir and Geiger, 2001a,b) The primary adhesion-mediating receptors in FA are heterodimeric (α and β) integrins, represented by the orange cylinders. For details concerning the various components, see (Geiger *et al*., 2001; Zamir and Geiger, 2001a,b). (B) Fluorescent microscopy of a 3T3 fibroblast adhering to an RGD-functionalized glass plate. F-actin stress fibers are shown in red and clusters of the ''plaque'' protein, vinculin is shown in green (overlapping areas are yellow). Vinculin marks the location of FA sites.

The desire for surfaces to provide information on the nanometer scale is given by the fact that major players of FA are proteins with dimensions in the range of several nanometers such as integrin, talin, vinculin, paxillin, or α-actinin (see also Fig. 2A and B). In recent years, it has become more and more evident that these adhesion-associated proteins assemble into hierarchical and cooperative arrangements, although we do not understand the mechanism how synergetic interactions between adhesion-associated proteins regulate the assembly and signaling functions of FA. The assembly of integrins along the cell membrane is one of the first events observed during the formation of FA (Alberts *et al*., 1994). Integrins are heterodimeric adhesion receptors which interact noncovalently with the RGD (arginine-glycine-aspartate) motif on ECM proteins, such as fibronectin and vitronectin. Ligand-binding affinity is influenced by conformational changes of the integrin molecule in response to both the extracellular environment and interactions with the cytoplasmic proteins of FA (Xiong *et al*., 2002). Although the very first moments of adhesion must be essential for adhesion formation, only little is known how initial adhesive interaction activates single integrins and stimulates them to cluster formation (Cohen *et al*., 2006; Li *et al*., 2003). Notably, the projected area of an integrin hetrodimer is thought to be $\sim$25 nm^2. However, the density of integrin clusters can vary dynamically, even among cells attached to the same surface. For example, integrin density in focal complexes is usually approximately three times lower than that seen in FA (Ballestrem *et al*., 2001). In this respect, integrin density and cluster structure are of most interest to be correlated with adhesion development and the consequent cellular response (Lasky, 1997). The size of integrins and other FA-associated proteins determines the length scale for the experimental manipulation of FA assembly, namely, in the order of 10 nm. A systems biology approach is needed to determine the effects of multiple perturbations—molecular-genetic manipulations, pharmacological treatments, and/or modifications of the adhesive surface—on FA structure and function. Currently, novel techniques are being developed to control structural surface arrangements by means of precise molecular nanopatterning.

Accordingly, the design of an adhesive substrate with molecular precision must take into account this length scale of molecular dimensions as well as the packing density characteristics of molecules within FA sites. A straightforward approach to engineer such adhesive surfaces is to first synthesize fully nonadhesive surfaces where interaction of cells and proteins with surfaces is minimal. Specific adhesive epitopes can then be integrated into this nonadhesive background. This approach is quite powerful since it provides us with the ability to dissect the relationship among specific cellular responses to ligand presentation, the interaction of adhesion receptors with specific ligands, and the lateral positioning of single integrins along the substrate.

Cell adhesion studies at nanoscale resolution may be divided into two general categories: (1) research addressing the responses of cells to variations in substrate topography (Dalby *et al*., 2002a,b, 2003; Ebendal, 1976; Kemkemer *et al*., 2004) and (2) the responses of cells to chemical variations along the substrate, which

affect the specificity of the adhesive ligand and/or its distribution (Arnold *et al.*, 2004; Elbert and Hubbell, 2001; Maheshwari *et al.*, 2000).

Our aim, as implied in the title of this chapter, is to discuss novel approaches for the *molecular engineering* of adhesive surfaces—referred to as ''nano-digital surfaces''—by means of chemical surface nanopatterning. Such artificial surfaces should be designed to allow individual control of their molecular composition and multiple physical features over a wide range of scales, from micro- down to nanometer levels without implying topographic features in surfaces to which cells do respond. Micro- and nanometer topographic corrugations in surfaces (Dalby *et al.*, 2002a,b, 2003; Ebendal, 1976; Kemkemer *et al.*, 2004) demonstrated that patterned surfaces may induce cell polarization and direct cell migration and that they may even regulate gene expression as well as cell signaling. Topographic features as small as 13 nm exert major effects on cell spreading, morphology, cytoskeletal organization, and even altering the cell's gene expression profile. Topographic features are avoided by, for example, plane film formation of polymers. Mixing signaling molecules with a biologically inert polymer such as polyethylene glycol (PEG) in combination with film formation (Elbert and Hubbell, 2001) as well as the use of oligo(ethylene oxide) functionalized self-assembled monolayers (SAMs) (Mrksich and Whitesides, 1997; Wang *et al.*, 1997) enabled the testing of cell responses to defined concentrations of signaling molecules.

Cell attachment to such passivated surfaces depends on many factors, such as the affinity and specificity of the corresponding cellular receptors for the ligand, the mechanical strength of ligand support and linkage, spacer length, overall ligand concentration, and spacing between ligand molecules (Roberts *et al.*, 1998). For example, the number of attached cells is clearly correlated to the average RGD surface density, as shown by the sigmoidal increase in attached cells with RGD concentration (Kantlehner *et al.*, 2000). This indicates that there is a minimal threshold ligand density for stable cell binding. In addition, it was found that, as a general rule, higher RGD surface density leads to an increase in cell spreading (up to a maximum), cell survival, and FA formation. It has also been established that the number of RGD molecules required for cell attachment is smaller than that needed for the induction of cell spreading and FA assembly. Furthermore, quantification of the average ligand density indicated that a threshold amount of as low as 6 (GRGDY) ligands/μm^2 is sufficient for maximal cell spreading, while $\sim$60 (GRGDY) ligands/μm^2 are needed for FA and stress fiber formation (Massia and Hubbell, 1991). Subsequent work with monolayer-coated surfaces suggested that a much higher density of ligands ($>$1000 RGD/μm^2) is required for maximum spreading of cells (Roberts *et al.*, 1998). Therefore, different biological responses exhibit different dependencies on ligand density.

Macromolecular designs, such as PEG stars, enable control over ligand homogeneity at the nanoscale. An average of 0, 1, 5, or 9 YGRGD ligands per star can be prepared, as demonstrated by Griffith and Lauffenburger in a series of publications (Elbert and Hubbell, 2001; Irvine *et al.*, 2001a,b; Koo *et al.*, 2002; Maheshwari *et al.*, 2000). Another advantage of the macromolecular approach is

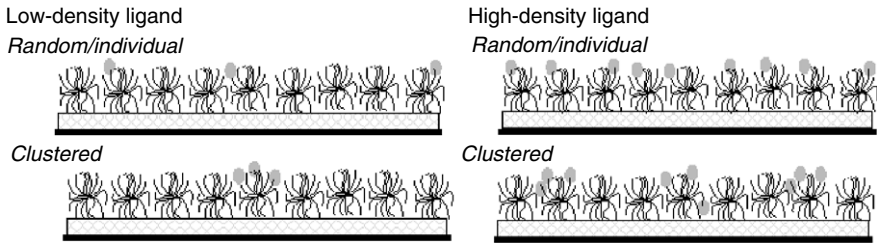

Fig. 3 Schematic illustration of star polymer as a tether to present ligands (shaded oval) in a manner in which the total average concentration (top vs bottom) and the spatial distribution, from homogeneous to highly clustered (left to right) can be independently varied (from Maheshwari *et al*., 2000).

that the long and flexible chain arms may facilitate cell-binding activities by allowing local rearrangement of ligands at the cell membrane. However, such flexibility is unlikely to induce precise molecular ligand clustering. The interaction enables ligands to cluster either by pure chemical affinity or following cellular rearrangement (Koo *et al*., 2002). Possible configurations for ligand patterns and local densities for two different macromolecular settings are shown in Fig. 3.

Precisely defined spatial distributions of ligands on an otherwise inert substrate could in principle shed light on many biological questions associated with matrix adhesion, formation, and cell signaling. A deeper understanding of how cell adhesion and signaling depend on the composition, size, and distribution of specific adhesion sites has remained elusive since most such studies have thus far been limited to micrometer or submicrometer areas (Sniadecki *et al*., 2006). However, surfaces patterned with both adhesive and non-adhesive domains by means of microcontact printing have been prepared (Gates *et al*., 2005; see Chapter 19), and successfully applied to geometrically control cell shape and viability on flat surfaces (Chen *et al*., 1997). These experiments strongly indicate that cell shape and integrin distribution can control the survival or apoptosis of cells and can also "switch on" and "switch off" specific gene expression programs.

II. Nano-Digital Chemical Surfaces for Regulating Transmembrane–Receptor Clustering

A. Extended Nanopatterns and Biofunctionalization

Precise control of defined spacing between adhesive ligands on interfaces at a length scale of 10–200 nm remains a major challenge. However, it is this length scale on which protein clustering at FA occurs, thus surface patterning at this length scale is highly relevant to cell physiology. Most recently, nanopattern features have been found in adhesive fibers of collagen (Jiang *et al*., 2004; Pompe *et al*., 2005), which are major adhesive components of the natural ECM as already discussed above (see also Fig. 1).

Micelle diblock copolymer lithography technology represents a nanopatterning strategy that enables the modification of substrates at this length scale. This approach is based on the self-assembly of diblock copolymers of polystyrene-block-poly (2-vinylpyridine) (PS-b-P2VP) into reverse micelles in toluene (Glass *et al.*, 2003a,b; Spatz *et al.*, 1996a,b,c, 2000). Diblock copolymers consist of two blocks of polymers joined by a covalent bond. The core of the micelle consists of the P2VP block complexed with a metal precursor ($HAuCl_4$), which is added to the micellar solution during preparation. Dipping and retracting a substrate from such a solution results in uniform and extended monomicellar films on the substrate (Fig. 4A), and subsequent treatment of these films with oxygen or hydrogen gas plasma results in the deposition of highly regular Au nanoparticles. The gold "dots" form a nearly perfect hexagonal pattern on solid interfaces such as glass or silicon (Si) wafers (Fig. 4F). The size of the Au nanoparticles may be varied between 1 and 20 nm by adjusting the amount of $HAuCl_4$ added to the micellar solution. The spacing between Au nanoparticles may also be adjusted from 15 to 250 nm, by choosing the appropriate molecular weight of PS-b-P2VP and by changing the retraction speed. A preparation scheme is presented in Fig. 4A.

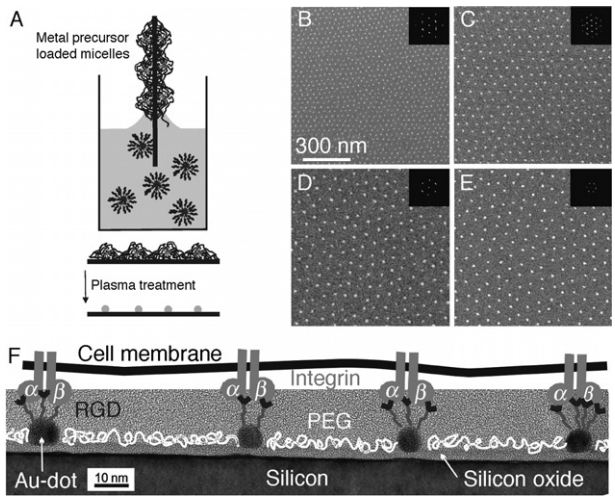

Fig. 4 Micellar block copolymer lithography and biofunctionalization. (A) Scheme of diblock copolymer micelle lithography. (B–E) Extended Au nanodot patterns are displayed by SEM. Uniform Au nanodots (bright spots) of (B) 3 nm by PS(190)-b-P[2VP$(HAuCl_4)_{0.5}$](190), (C) 5 nm by PS(500)-b-P[2VP$(HAuCl_4)_{0.5}$](270), (D) 6 nm by PS(990)-b-P[2VP$(HAuCl_4)_{0.5}$](385), and (E) 8 nm by PS(1350)-b-P[2VP$(HAuCl_4)_{0.5}$](400) deposited onto Si-wafers are shown. The number in brackets refers to the number of monomer units in each block which control the separation between Au dots. These varied between (B) 28, (C) 58, (D) 73, and (E) 85 nm. The Au dots form extended, nearly perfect hexagonally close-packed patterns as indicated by the Fourier transform images (inset) which show second order intensity spots. (F) Biofunctionalization of the Au nanodots pattern (Arnold *et al.*, 2004). Since the Au dot is sufficiently small, it is most likely that only one integrin transmembrane receptor directly interacts with one dot. The Au dots are presented as side view micrographs taken with a high-resolution transmission electron microscope (adapted from Arnold *et al.*, 2004).

SEM images of Si wafers coated with these Au nanoparticles show Au nanoparticles as white spots arranged in quasi-hexagonal patterns (Fig. 4B–E). The patterns consist of Au nanoparticles 3, 5, 6, or 8 nm in diameter with spacings of 28, 58, 73, and 85 nm, respectively, between dots. A side view of the Au nanodots, taken by means of high-resolution transmission electron microscopy, is shown in Fig. 4F. These nanostructures serve as chemical templates for the spatial arrangement of RGD-based ligands, as shown schematically in Fig. 4F (Arnold *et al.*, 2004).

Passivation of the interface entails the binding of a polyethylene oxide (PEO) layer to the silicon oxide or glass substrate, covering the surface between the Au nanodots to avoid any interaction of the surface with proteins or the cell membrane. Subsequently, the Au dots are functionalized by the adhesive ligands that bind selectively to the Au nanoparticle. Cyclic RGD molecules (c(RGDfK)-thiol) recognized with high affinity by $\alpha v\beta 3$-integrin (Haubner *et al.*, 1997; Pfaff *et al.*, 1994) have been used successfully (Arnold *et al.*, 2004). In Fig. 4F, Au dots and integrins are drawn approximately to scale, indicating that the size of an Au nanodot provides a molecular anchor of a size that only a single integrin is likely to bind to. These nanodots thus constitute a very valuable tool to provide unique access to an important length scale for cell adhesion studies and allow to control the assembly of single integrins during the formation of FA clusters.

It is noteworthy that there are wide choices of ligands to link to the Au dots and different immobilization procedures are applicable for each ligand. Straightforward coupling of ligands to Au nanoparticles is enabled by molecules or proteins with a thiol (−SH) group, for example, through a cysteine residue. Other possibilities include binding a carboxylic acid group (−COOH) to Au nanostructures which can then be activated by carbodiimides and covalently linked with amine groups. Since amine groups are commonly distributed in proteins, oriented immobilization is usually lacking. However, His-tagging, using either a synthetic or molecular genetic approach, is now coming into wide use, enabling oriented immobilization of nearly any ligand. Oriented binding of peptides or proteins to the Au nanoparticles has been achieved using $(His)_6$-tagging, which binds to NTA via nickel ion complexation. Lately, the stability of His-tag–NTA Ni complexes has been substantially improved by introducing multivalent complexation (Lata and Piehler, 2005). A biotin tag genetically engineered into a molecule can also be exploited as a linker for oriented binding of the molecule to surfaces, via a series of linkages mediated by streptavidin, for example (molecule-biotin)-streptavidin-(biotin-surface).

B. Micro-Nanopatterns for Spatially Controlled Molecular Clustering

In order to arrange locally a defined number of Au nanoparticles in a designated pattern, extended monomicellar layers are directly exposed to a focused ray of light in a conventional mask aligner or to an electron beam (e-beam) in an SEM. Either method will chemically modify the polymer located in exposed areas (Glass *et al.*, 2003a,b). This process is depicted in Fig. 5A. Locally exposed layers are washed in

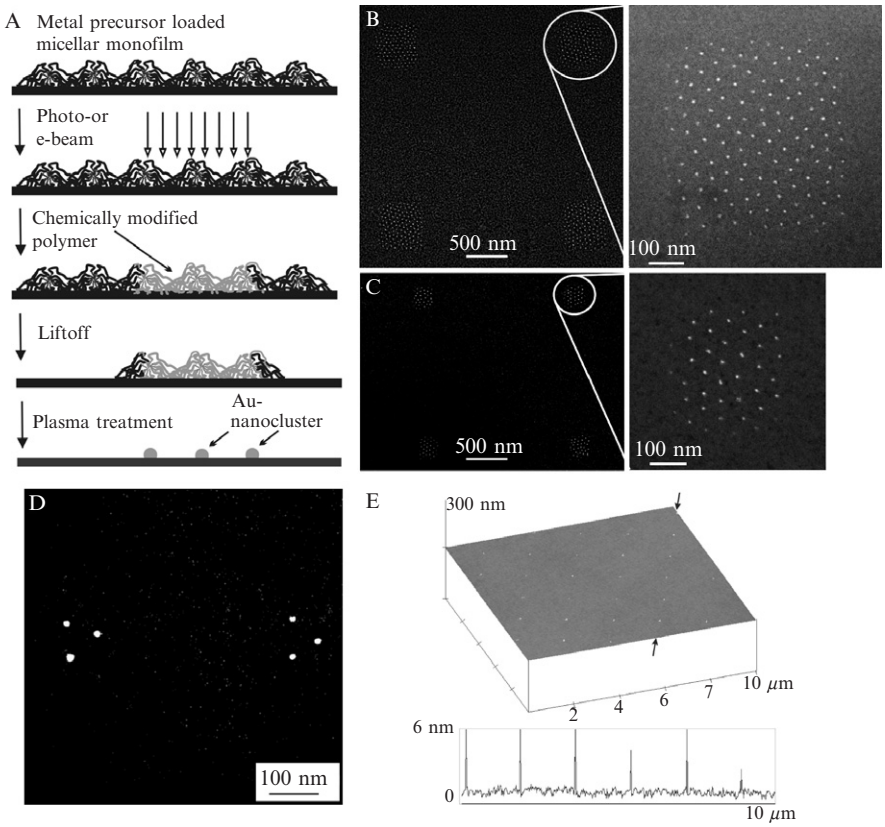

Fig. 5 (A) Application of monomicellar films as negative e-beam resist. The complementary length scales of a diblock copolymer micelle in which a single nanodot is perfectly positioned in the center and the resolution of photo- or e-beam lithography which reaches the diameter of a diblock copolymer micelle make this concept a suitable technology for the inexpensive generation of various micro-nanopatterns; for example, (B) squares made of ~100 × 6 nm Au particles, (C) squares made of ~40 × 6 nm Au particles, (D) 3 × 6 nm Au particles separated by ~400 nm, (E) single 6-nm Au particle separated by 2 μm in a square pattern (adapted from Glass *et al.*, 2003a,b).

dimethylformamide (DMF) or toluene in an ultrasound bath, and the remaining micelles are treated with gas plasma, resulting in the deposition of a pattern of nanoscopic Au particles in designated areas.

The SEM micrographs pictured in Fig. 5B–D show 6-nm Au particles localized within squares, each with ~100, 40, or 3 Au particles. Figure 5E shows a SEM image of single 6-nm Au particles separated by ~2 μm, arranged in a square pattern. Assuming that each Au nanoparticle represents a binding site for individual molecules, this method allows the size of ligand clusters to be controlled and quantified.

In the above procedure, the underlying surface had to be gas plasma resistant, which excludes the use of polymer surfaces as nanopattern supports. However, developments show that one can transfer such patterns to almost any type of soft surfaces (Fig. 6) (Graeter *et al.*, 2007), equipping one side of the gold dot surface area with a photosensitive linker molecule which then binds covalently to a polymer cast on top of the array. Pealing-off the polymer from the surfaces which originally carried the gold dots results in a complete transfer of the dots to the polymer matrix. This discovery is a major step forward in nanopattern substrate preparation since it enables the stiff glass or silicon oxide surfaces to be replaced with elastic or viscoelastic polymer surfaces. This new approach is regarded important for controlling surface properties that impact on cellular responses.

Figure 7A–C shows scanning electron micrographs of gold nanostructures 6 nm in size, represented as white spots on substrates made of either PS (A), PDMS (B), or PEGDA 20,000 hydrogels. Figure 7C represents a cryoscanning electron micrograph of a PEG hydrogel frozen in the water-swollen state at approximately −120 °C. Independently of the polymer, the nanostructures were successfully transferred one-to-one, with nanoscale precision, from the glass to the respective polymer substrate. These results demonstrate that transfer lithography is applicable to various polymers from rigid hydrophobic polystyrene to elastic silicone to soft hydrogels.

Another challenge for nanofabrication techniques is to prepare nanopatterns beyond planar surfaces. Curved surfaces are obviously meaningful for studies of cell behavior because most cells are three-dimensionally embedded in the ECM. This study confirms the feasibility of the block copolymer micelle nanolithography

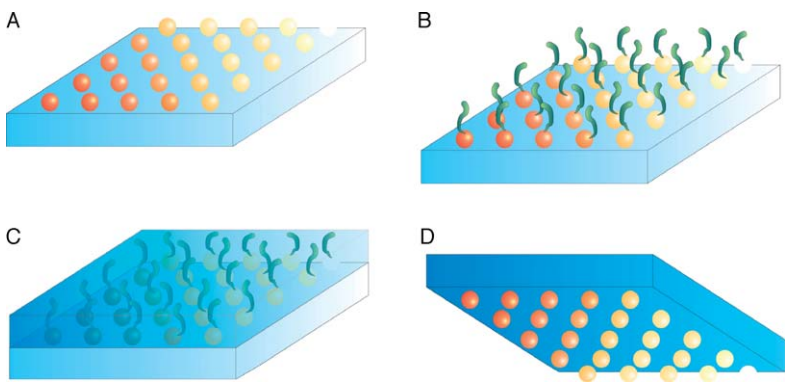

Fig. 6 Schematic presentation of the transfer nanolithography (Graeter *et al.*, 2007). (A) Gold nanostructures are deposited on glass supports by means of diblock copolymer micelle nanolithography, followed by chemical functionalization through linker molecules (B). (C) Coating of the glass support by a polymer and mechanical separation of the inorganic support and the polymer layer which transfers the inorganic structures from the glass to the polymer support (D).

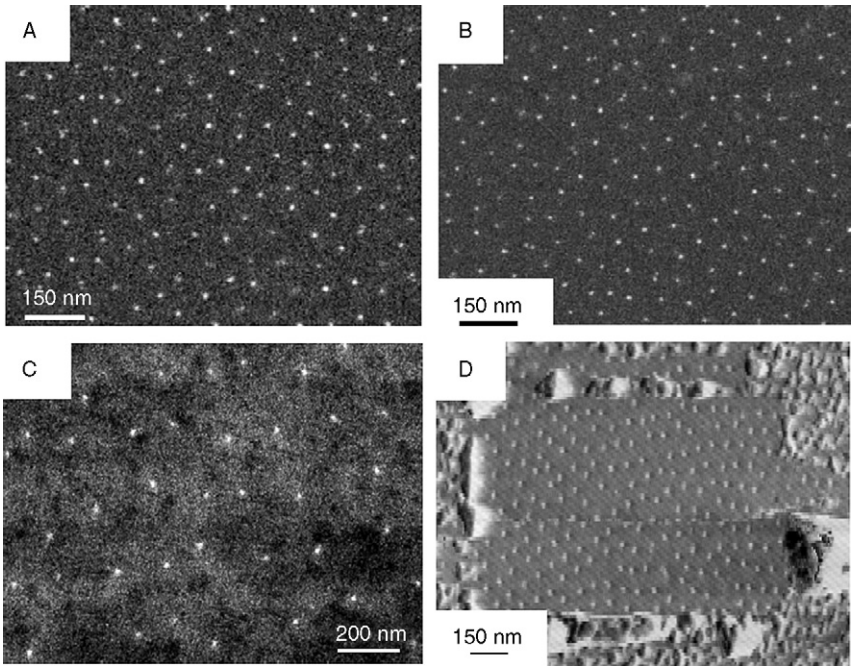

Fig. 7 Gold nanostructures on various polymer substrates as patterned by transfer lithography (Graeter *et al.*, 2007). SEM images of gold nanoparticles transferred from glass to PS (A) and PDMS (B). (C) A cryo-scanned electron micrograph of a gold nanopattern on a PEGDA 20,000 hydrogel. (D) Atomic force microscopy (AFM) micrograph of gold nanoparticles on a PEGDA 700 hydrogel immersed in water (Graeter *et al.*, 2007).

technique for nonplanar surfaces. As a demonstration, a tubelike hydrogel with a nanopatterned internal surface was prepared.

The diblock copolymer micelle nanolithographic technique was extended so as to decorate glass fibers with gold nanoparticles. Accordingly, glass fibers with diameters ranging from 60–500 μm were coated with nanostructures by dip-coating, as described for the planar substrates. The fibers were then treated with a hydrogen plasma to remove the micellar diblock copolymer from the gold particles as well as the glass fiber and to deposit the gold nanoparticles along the fiber. The remaining metal particles showed a typical hexagonal arrangement like that seen on the planar substrates (Fig. 8A). As with the transfer process of particles to a planar substrate, the gold particles were functionalized with a linker molecule. After embedding the fibers in PEGDA 700 and cross-linking PEGDA (Fig. 8B, step 1), the glass fiber was dissolved with hydrofluoric acid (Fig. 8B, step 2). This yielded channel structures internally decorated with gold nanoparticles (Fig. 8D), as revealed by cryo-SEM of frozen and halved channels (Fig. 8C and D).

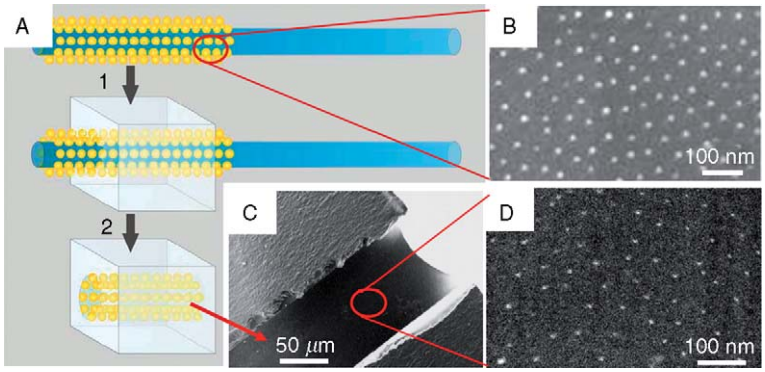

Fig. 8 Formation of nanostructured hydrogel microtubes (Graeter *et al.*, 2007). (A) Schematic drawing of the transfer lithography technique applied to curved surfaces, for example optical fibers. (B) SEM micrograph of a glass fiber decorated with gold nanoparticles by means of block copolymer micelle nanolithography. (C and D) Cryo-SEM images of a PEGDA 700 hydrogel channel decorated with gold nanoparticles.

C. Cellular Responses to Nano-Digital and Biofunctionalized Surfaces

Given the ability to functionalize adhesion surfaces with nanoscale resolution, one can test the diverse cellular responses to such patterns. In Fig. 9, MC3T3 osteoblasts were seeded on glass coverslips and examined by phase contrast microscopy. Only part of the glass substrate area was patterned with Au nanodots separated by different distances. The Au dots were functionalized by c(RGDfK)-thiols and the surrounding glass surface was passivated by PEG.

When plated on functionalized Au nanodot patterns separated by varying widths, MC3T3 osteoblasts display varied adhesive behaviors. It is evident that cells spread very well on the 58-nm pattern (Fig. 9A), comparable to their spreading on uniform RGD- or fibronectin-coated surfaces (data not shown). On the other hand, very limited cell spreading is observed on substrates with Au nanodots spaced 73 nm or more apart (Fig. 8B). Stationary cells appear rounded, while migrating cells are usually characterized by long extensions. Similar observations were made with other cell types, including REF52 fibroblasts, 3T3 fibroblasts, and B16 melanocytes.

Cell studies on nanostructured PEG hydrogels gold nanoparticles were transferred to PEG hydrogels and functionalized by cyclic RGDfK peptides. The gold nanostructured hydrogels were incubated in a 0.2-mmol solution of the cyclic RGDfK-thiol in water for 1 h. The hydrogels were then intensively washed with water to remove peptides which might have penetrated the gel. Subsequently, 3T3 fibroblasts were cultured for 24 h under standard cell culture conditions (in DMEM with 1% FBS) on PEGDA 700 hydrogels equipped with gold nanoparticles separated by distances of 40 nm. Figure 10A shows gold nanostructures that were not functionalized by cyclic RGDfK. Only a few cell aggregates are visible in

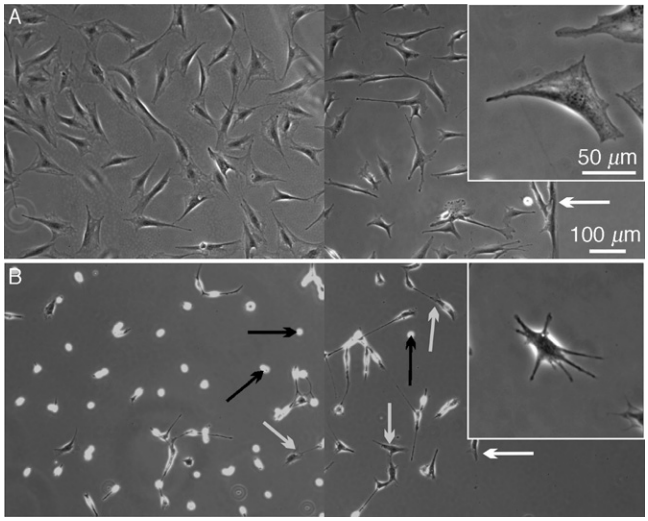

Fig. 9 Phase contrast microscopy of MC3T3-Osteoblasts attached to nanopatterned surfaces of different spacings: (A) ~58 and (B) ~73 nm. The right side was entirely passivated; thus, cell adhesion and attachment are only observed on the left side of the images. A line of cells marks the borderline of the nanopatterned area (white arrows). It is evident that cells spread very well on the 58 nm (Fig. 9A insert) pattern, comparable to their spreading on uniform RGD- or fibronectin-coated surfaces (not shown). On the other hand, very limited cell spreading is observed on substrates with 73-nm-spaced nanodots (Fig. 9B, insert). Stationary cells (black arrows) appear rounded, while migrating cells (gray arrows) are usually characterized by long extensions. Similar observations were made with other cell types, including REF52 fibroblasts, 3T3 fibroblasts, and B16 melanocytes (adapted from Arnold *et al.*, 2004).

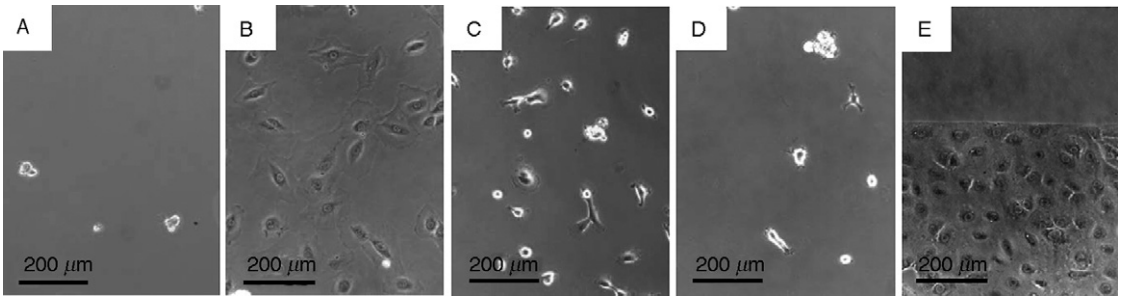

Fig. 10 Phase contrast optical micrographs of 3T3 fibroblasts on PEGDA 700 hydrogels. (A) Cells on a non-RGD-functionalized gold nanoparticle pattern. (B–D) Cells on cyclic RGDfK-functionalized gold particles; cyclic RGDfK patches are separated by varying distances (B) 40 nm, (C) 80 nm, and (D) 100 nm, after 24 h in culture. (E) Dense cell layer on a PEG support after 14 days in culture. The bottom part of the sample was patterned with cyclic RGDfK peptide-functionalized gold nanoparticles spaced 40 nm apart (adapted from Graeter *et al.*, 2007).

Fig. 10A, which indicates that cells neither spread nor survive. After functionalization of the gold nanostructures with cyclic RGDfK, cell attachment and spreading are clearly visible in Fig. 10B. Cells did not spread on the undecorated hydrogel, rather only on areas with gold particles, as illustrated by the partially gold-decorated substrate in Fig. 10E. With this substrate, the long-term biological activity of the gold-decorated hydrogel was investigated by culturing fibroblasts for more than 14 days on a PEGDA 700 hydrogel partially decorated with cyclic RGDfK-functionalized gold particles. A dense layer of cells was observed only in the region with a cyclic RGDfK-functionalized nanopattern. In agreement with previous studies of nanopatterned glass surfaces as shown in Fig. 9 (Arnold *et al.*, 2004), cell adhesion and spreading failed if cyclic RGDfK functionalized gold nanoparticles were separated by a critical distance near 80 nm (Fig. 10C). In the case of larger distances (Fig. 10D), cells could attach to the functionalized nanodots but efficient cell adhesion and spreading did not happen. Our preliminary cell experiments illustrate that our nanolithography technique is biocompatible, and the results meanwhile imply effects of cell adhesion on the nanopatterned polymer surfaces.

In order to make the inside of the PEG hydrogel microchannels adhesive for cells, the tube was further biofunctionalized by a 0.2-m*M* water solution of cyclic RGDfK which was injected with a syringe into the channel; the microchannels were then incubated for 1 h. After the microchannels were intensively rinsed with water, HeLa cells were seeded into the channel and cultured under standard conditions for 24 h. Figure 11E and F depict cell spreading along the nanopatterned interior wall of the hydrogel tubes.

The molecular requirements for the formation of FA and the assembly of actin stress fibers in MC3T3 osteoblasts were further investigated by culturing these cells for 1 day, then fixing and staining them for the presence of vinculin and actin. Figure 12 shows fluorescence confocal micrographs of cells attached to c(RGDfK)-coated Au dots with spacings of (A) 58 nm and (B) 73 nm. It is apparent that an Au nanodot separation of 58nm induces the formation of large vinculin-rich FA and well-defined actin stress fibers, compared to the poorly organized vinculin and actin structures on nanodots separated by 73 nm (B) or more.

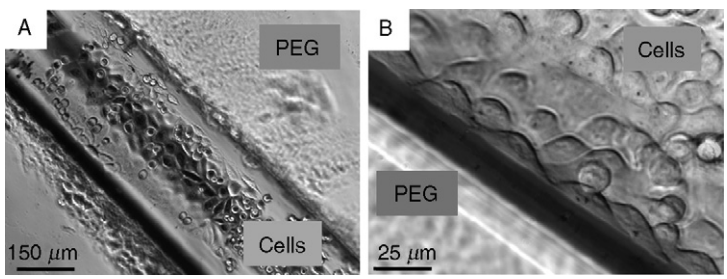

Fig. 11 (A and B) HeLa cells cultured in PEGDA 700 hydrogel tubes functionalized with RGDfK-functionalized gold nanoparticles (adapted from Graeter *et al.*, 2007).

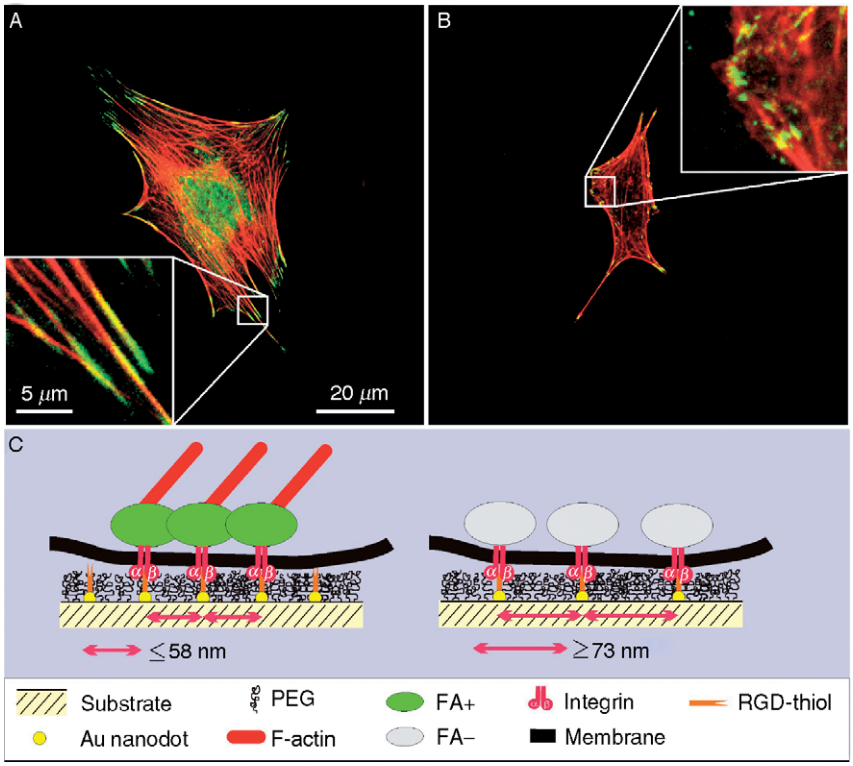

Fig. 12 Pair of confocal fluorescent micrographs of MC3T3 osteoblasts stained for vinculin (green) and actin (red) (Arnold *et al*., 2004). Cells interacting with Au nanodot patterns with Au dot spacing of (A) 58 nm and (B) 73 nm. (C) Scheme depicting a hypothetical model that can explain the differential effects of the 58- and 73-nm-spaced, biofunctionalized nanopattern on integrin clustering and cytoskeletal organization. According to this model, a separation of Au/RGD dots by >73 nm causes limited cell attachment and spreading and actin stress fiber formation due to immobilization of integrin at intermolecular distances which are incompatible with transmembrane induction of FA formation. Intermolecular distances of <58 nm allow for such transmembrane interactions to take place, resulting in efficient FA formation (adapted from Arnold *et al*., 2004).

D. Local Versus Global Effects of Ligand Density on Cell Adhesion

Surfaces bearing nanopatterns with different spacings also present different absolute numbers of nanodots per unit area to the attached cells. To determine whether the differential cellular responses to such surfaces might be attributable to the dot-to-dot distances (referred to as the local ligand density) or to the total number of nanodots present at the cell-surface interface (referred to as the global ligand density), the "micro"-nanostructured surfaces, prepared as described above (Glass *et al*., 2003a,b), were used to deposit a fixed number of Au nanodots confined to a "micropatch" on the substrate. The surfaces were designed such

that the global dot density was 90 dots/μm^2, thus significantly lower than either case of extended Au dot patterns, where the density was 280 dots/μm^2 for Au dots separated by 58 nm and 190 dots/μm^2 for Au dots separated by 73 nm. The local dot density present in 2×2 μm^2 patches of 58-nm-spaced dots was still 280 dots/μm^2 (Fig. 13A). A bright-field optical micrograph, taken 3 h after the plating of MC3T3 osteoblasts on the substrate, indicates that cells are confined to the structured area as the process of cell spreading advanced (Fig. 13B, inset). Twenty-four hours later, well-spread cells could be seen in this area (Fig. 13C), whereas cells located outside the frame spread poorly. A confocal fluorescent micrograph of a cell stained for vinculin and actin demonstrates the confinement of FA to the square micropattern and the association of the termini of actin stress fibers at these sites (Fig. 13D). The size distribution in FA lengths is remarkably narrow, indicating its confinement to the functionalized square.

These adhesion experiments indicate that local dot-to-dot separation (namely, local ligand density), rather than the global ligand number, is critical for inducing

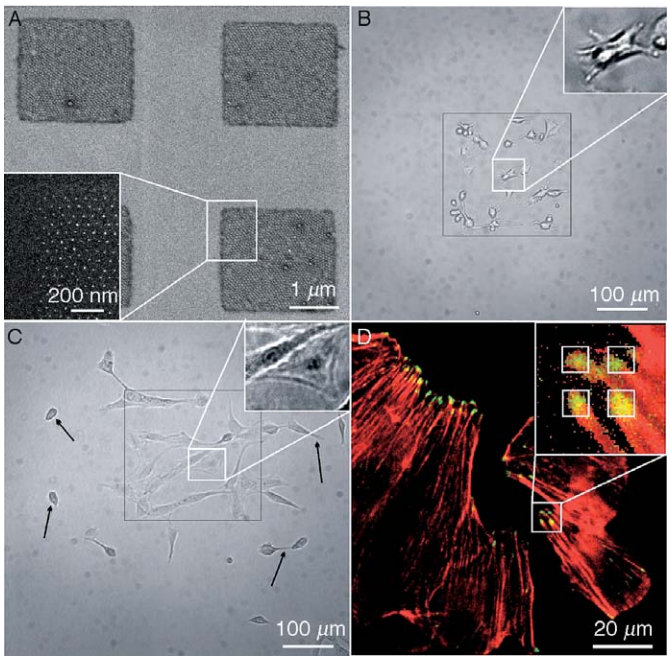

Fig. 13 MC3T3-osteoblast adhesion on "micro"-nanostructures functionalized by c(RGDfK)-thiols. (A) SEM image of "micro"-nanostructures: SEM micrograph of 5-nm Au dots separated by 58 nm in a hexagonally close-packed pattern, localized in 2×2 μm squares which are separated by 1.5 μm. Bright-field optical micrograph of adhesive MC3T3-osteoblasts growing on the pattern shown in (A), covering the area in the marked box. Cells were cultured for 3 h (B) or 24 h (C). (D) Fluorescence optical micrograph of MC3T3-osteoblast showing the location of FA by fluorescent staining for vinculin (green) and actin (red)(adapted from Arnold *et al.*, 2004).

cell adhesion and FA assembly. Thus, for example, the global dot density of "micro"-nanostructured squares with 58-nm spacing is considerably lower than that of substrates uniformly patterned with dots at a spacing of 73 nm or more. Nevertheless, cells did form FA on the former surface and failed to do so on the latter surface. These findings are schematically summarized in Fig. 12C.

In future studies, the micro-nanopattern technique will allow for even larger variations in the organization of nano-adhesive sites. This will include alterations in ligand template pliability and presentations of small dot clusters—for example, pairs or triplets—which may shed light on the minimal molecular number that defines an effective integrin cluster for supporting cell attachment, spreading, or migration. It will also allow the exploration of pattern-specific features (i.e., molecularly defined adhesion "cues") that trigger cell adhesion-based signaling (Arnold *et al.*, 2004).

E. Cell Spreading and Migration on Different Nanopatterns

The difference in nanopattern spacing clearly affects the extent of cell spreading (measured as projected cell area). As shown in Fig. 14, the projected cell area is dramatically reduced on surfaces with an interparticle spacing $d > 73$ nm, supporting the notion that cell spreading is an active process triggered by specific (and density-dependent) integrin signals. Furthermore, dynamic analysis revealed the instability of FA in cells attached to the sparse RGD-nanopattern, associated with an increased migratory activity of cells (data not shown).

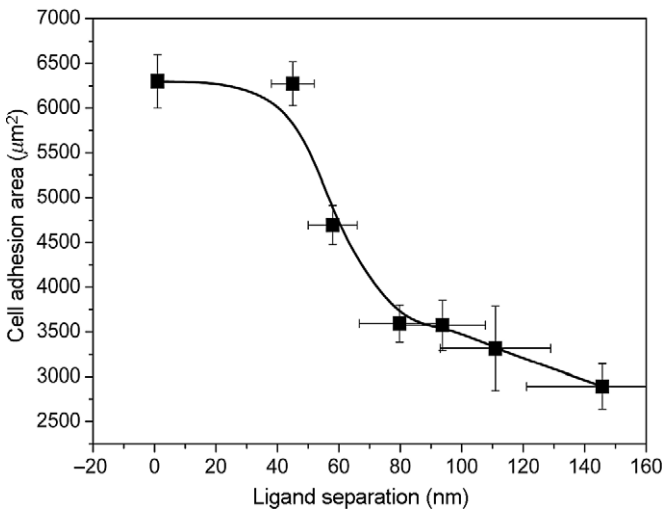

Fig. 14 Projected cell adhesion area per cell adhering to different ligand (dot) separation.

F. High-Resolution Visualization of Cells in Contact with Biofunctionalized Nanopatterns

Conventional optical microscopy is limited in spatial resolution to >200 nm, and thus cannot resolve individual adhesion points on nanopatterned surfaces. SEM was therefore utilized to visualize individual adhesions. Figure 15 shows a series of SEM micrographs, which illustrate cells attached to micro-nanopatterns (Fig. 15A and B) and to extended nanopatterns (Fig. 15C). The local interdot spacing was 58 nm in all samples. Nanoprotrusions attached to individual nanodots could be seen (Fig. 15C). Examination of a large area along the surface indicated that the lamellipodium attaches to the micro-nanopattern "islands," rather than to the surrounding passivated area. A high-resolution micrograph illustrates the interaction of a cell protrusion with the nanopattern (Fig. 15C). The tiny nanoscopic membrane protrusions attach selectively to the RGD-functionalized Au nanoparticles and not to the PEG-passivated glass.

The latter observation is remarkable since it directly displays cellular adhesive nanostructures formed in response to molecularly defined interactions. The tiny

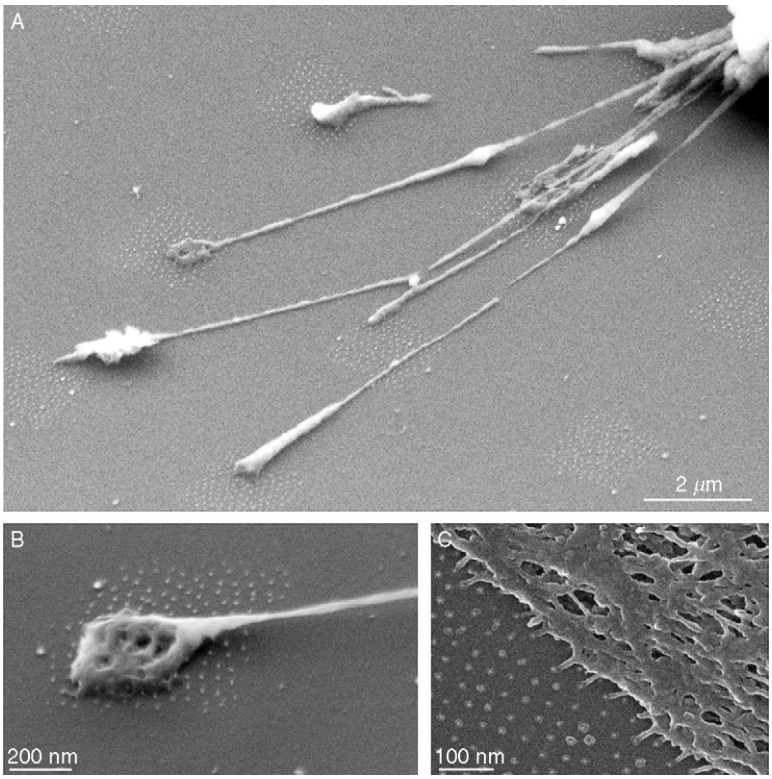

Fig. 15 SEM micrographs displaying 3T3 fibroblast adhering to micro-nanopattern (A and B) and to extended nanopattern (C). The dot spacing was 58 nm in all samples (adapted from Arnold *et al.*, 2004).

membrane protrusions may be as small as 20 nm in diameter and are most likely anchored to the adhesive nanoparticles (due to space restriction on each dot) via single-integrin molecules located at the tip of the membrane.

III. Outlook for the Future

Recent efforts to systematically control multiple features of adhesive substrates have greatly benefited from advanced research in materials science. The long-term objective of this effort is to design and fabricate so-called "cellular environments" with defined chemical and physical properties in order to exert desirable effects on cell structure, activity, and fate. Self-assembled micelle diblock copolymer nanolithography and other associated biofunctionalization approaches described herein represent a new era in the development of tailored cellular environments, in which both the chemical and physical features can be exquisitely controlled with high, molecularly defined precision. For this reason, we refer to the design of such "biointerfaces" as "molecular engineering," and to the surfaces themselves as "nano-digital interfaces."

The most recent data show that surface variations at the nanoscale range, namely the typical size of single-protein complexes, can be sensed by cells and dramatically affect their behavior. This knowledge may be further expanded by combining such variations with manipulations of other properties of the adhesive surface such as topography, isotropy, rigidity, and texture. The replacement of rigid glass substrates as a support for nanoparticles by more flexible polymer surfaces is a major step forward in this regard (Graeter *et al.*, 2007). The use of polymers as substrate not only allows for chemically nanopatterned surfaces of varying elasticity and viscoelasticity, even at microdimensions, but also presents a new challenge as one attempts to shape chemically nanopatterned surfaces in different ways (e.g., fabrication of nanopatterned supports in tube shapes for artificial vessels or stents or in other three-dimensional configurations). These novel substrates may ultimately modulate receptor presentation, occupation, and immobilization at the cell membrane, as well as alter the transcriptional program which, in turn, may affect multiple signaling events and cellular responses such as cell dynamics, differentiation, and fate.

Acknowledgments

This work has been made possible by a number of excellent students, postdocs, and colleagues from our groups, namely Dr. Ada Cavalcanti-Adam (MPI-MF & Uni Heidelberg), Dr. Marco Arnold (MPI-MF & Uni Heidelberg), Dr. Jacques Blümmel (MPI-MF & Uni Heidelberg), Dr. Roman Glass (MPI-MF & Uni Heidelberg), Nadine Perschmann (MPI-MF & Uni Heidelberg), Dr. Stefan Gräter (MPI-MF & Uni Heidelberg), Dr. Baruch Zimerman (Weizmann Institute), and Dr. Tova Volberg (Weizmann Institute). The RGD peptides were kindly provided by Professor Horst Kessler, TU Munich. The collaboration between B.G. and J.S. is supported by the Landesstiftung Baden-Württemberg, by the German-Israeli Foundation, and by the Max Planck Society. B.G. holds the Erwin Neter Professorial Chair in Cell and Tumor Biology.

References

Alberts, B., Bray, D., Lewis, J., Raff, M., Roberts, K., and Watson, J. D. (1994). ''Molecular Biology of the Cell,'' 3rd edn. Garland Publishing, New York, USA.

Alberts, B., Johnson, A., Lewis, J., Raff, M., Roberts, K., and Walter, P. (2001). ''Molecular Biology of the Cell,'' 4th edn. Garland Science, New York, USA.

Arnold, A., Cavalcanti-Adam, A., Glass, R., Blümmel, J., Eck, W., Kessler, H., and Spatz, J. P. (2004). Activation of integrin function by nanopatterned adhesive interfaces. *Chemphyschem.* **3,** 383–388.

Balaban, N. Q., Schwarz, U. S., Rivelin, D., Goichberg, P., Tzur, G., Sabanay, L., Mahalu, D., Safran, S., Bershadsky, A., Addadi, L., and Geiger, B. (2001). Force and focal adhesion assembly: A close relationship studied using elastic micropatterned substrates. *Nat. Cell Biol.* **3,** 466–472.

Ballestrem, C., Hinz, B., Imhof, B. A., and Wehrle-Haller, B. (2001). Marching at the front and dragging behind: Differential alphaVbeta3-integrin turnover regulates focal adhesion behavior. *J. Cell Biol.* **155,** 1319–1332.

Blau, H. M., and Baltimore, D. J. (1991). Differentiation requires continuous regulation. *J. Cell Biol.* **112,** 781–783.

Chen, C. S., Mrksich, M., Huang, S., Whitesides, G. M., and Ingber, D. E. (1997). Geometric control of cell life and death. *Science* **276,** 1425–1428.

Critchley, D. R. (2000). Focal adhesions—the cytoskeletal connection. *Curr. Opin. Cell Biol.* **12,** 133–139.

Cohen, M., Kam, Z., Addadi, L., and Geiger, B. (2006). Dynamic study of the transition from hyaluronan- to integrin-mediated adhesion in chondrocytes. *EMBO* **25**(2), 302–311.

Dalby, M. J., Yarwood, S. J., Riehle, M. O., Johnstone, H. J. H., Affrossman, S., and Curtis, A. S. G. (2002a). Increasing fibroblast response to materials using nanotopography: Morphological and genetic measurements of cell response to 13-nm-high polymer demixed islands. *Exp. Cell Res.* **276,** 1–9.

Dalby, M. J., Riehle, M. O., Johnstone, H. J. H., Affrossman, S., and Curtis, A. S. G. (2002b). *In vitro* reaction of endothelial cells to polymer demixed nanotopography. *Biomaterials* **23,** 2945–2954.

Dalby, M. J., Childs, S., Riehle, M. O., Johnstone, H. J. H., Affrossman, S., and Curtis, A. S. G. (2003). Fibroblast reaction to island topography: Changes in cytoskeleton and morphology with time. *Biomaterials* **24,** 927–935.

Discher, D. E., Janmey, P., and Wang, Y. L. (2005). Tissue cells feel and respond to the stiffness of their substrate. *Science* **310,** 1139–1143.

Ebendal, T. (1976). The relative roles of contact inhibition and contact guidance in orientation of axons extending on aligned collagen fibrils *in vitro*. *Exp. Cell Res.* **98**(1), 159–169.

Elbert, D. L., and Hubbell, J. A. (2001). Conjugate addition reactions combined with free-radical cross-linking for the design of materials for tissue engineering. *Biomacromolecules* **2,** 430–441.

Fratzl, P., Misof, K., Zizak, I., Rapp, G., Amenitsch, H., and Bernstorff, S. (1998). Fibrillar structure and mechanical properties of collagen. *J. Struct. Biol.* **122,** 119–122.

Gates, B. D., Xu, Q., Stewart, M., Ryan, D., Willson, C. G., and Whitesides, G. M. (2005). New approaches to nanofabrication: Molding, printing, and other techniques. *Chem. Rev.* **105**(4), 1171–1196.

Geiger, B., Bershadsky, A., Pankov, R., and Yamada, K. (2001). Transmembrane extracellular matrix cytoskeleton crosstalk. *Nat. Rev. Cell Biol.* **2,** 793–805.

Georges, P. C., and Janmey, P. A. (2005). Cell type-specific response to growth on soft materials. *J. Appl. Physiol.* **98,** 1547–1553.

Giancotti, F. G., and Ruoslahti, E. (1999). Integrin signaling. *Science* **285,** 1028–1032.

Glass, R., Arnold, M., Möller, M., and Spatz, J. P. (2003a). Micro-nanostructured interfaces fabricated by the use of inorganic block copolymer micellar monolayers as negative resist for electron beam lithography. *Adv. Funct. Mater.* **13,** 569–575.

Glass, R., Möller, M., and Spatz, J. P. (2003b). Block copolyer micelle nanolithography. *Nanotechnology* **14,** 1153–1160.

Graeter, S., Jinghuan, H., Perschmann, N., López, M., Kessler, H., Ding, J., and Spatz, J. P. (2007). Mimicking cellular environments by nónostructured soft interfaces. *Nano Lett.* **7**(5), 1413–1418.

Haubner, R., Finsinger, D., and Kessler, H. (1997). Stereoisomeric peptide libraries and peptidomimetics for designing selective inhibitors of the alpha(V)beta(3) integrin for a new cancer therapy. *Angew. Chem. Int. Ed.* **36**(13–14), 1375–1389.

Hynes, R. O. (1987). Integrins—a family of cell-surface receptors. *Cell* **48,** 549–554.

Irvine, D. J., Mayes, A. M., and Griffith, L. G. (2001a). Nanoscale clustering of RGD peptides at surfaces using comb polymers. 1. synthesis and characterization of comb thin films. *Biomacromolecules* **2,** 85–94.

Irvine, D. J., Ruzette, A. V. G., Mayes, A. M., and Griffith, L. G. (2001b). Nanoscale Clustering of RGD peptides at surfaces using comb polymers. 2. surface segregation of comb polymers in polylactide. *Biomacromolecules* **2,** 545–556.

Jiang, F. Z., Horber, H., Howard, J., and Müller, D. (2004). Assembly of collagen into microribbons: Effects of pH and electrolytes. *J. Struct. Biol.* **148**(3), 268–278.

Kantlehner, M., Schaffner, P., Finsinger, D. M. J., Meyer, J., Jonczyk, A., Diefenbach, B., Nies, B., Hölzemann, G., Goodman, S. L., and Kessler, H. (2000). Surface coating with cyclic RGD peptides stimulates osteoblast adhesion and proliferation as well as bone formation. *Chem. Bio. Chem.* **1,** 107–114.

Kemkemer, R., Schrank, S., Gruler, H., Kaufmann, D., and Spatz, J. P. (2004). Process of cell shape normalization of normal and haploinsufficient NF1-melanocytes through substrate interaction. *Chem. Phys. Chem.* **3,** 85–92.

Koo, L. Y., Irvine, D. J., Mayes, A. M., Lauffenburger, D. A., and Griffith, L. G. (2002). Co-regulation of cell adhesion by nanoscale RGD organization and mechanical stimulus. *J. Cell Sci.* **115,** 1423–1433.

Lasky, L. A. (1997). Cell adhesion: How integrins are activated. *Nature* **390,** 15–17.

Lata, S., and Piehler, J. (2005). Stable and functional immobilization of histidine-tagged proteins via multivalent chelator headgroups on a molecular poly(ethylene glycol) brush. *Anal. Chem.* **77**(4), 1096–1105.

Levenberg, S., Katz, B. Z., Yamada, K. M., and Geiger, B. (1998). Long-range and selective autoregulation of cell-cell or cell-matrix adhesions by cadherin or integrin ligands. *J. Cell Sci.* **111,** 347–357.

Li, R., Mitra, N., Gratkowski, H., Vilaire, G., Litvinov, R., Nagasami, C., Weisel, J. W., Lear, J. D., DeGrado, W. F., and Bennett, J. S. (2003). Activation of Integrin αIIbß3 by modulation of transmembrane helix associations. *Science* **300,** 795–798.

Lin, F., and Butcher, E. C. (2006). T cell chemotaxis in a simple microfluidic device. *Lab Chip* **6**(11), 1462–1469.

Maheshwari, G., Brown, G., Lauffenburger, D. A., Wells, A., and Griffith, L. G. (2000). Cell adhesion and motility depend on nanoscale RGD clustering. *J. Cell Sci.* **113,** 1677–1686.

Massia, S. P., and Hubbell, J. A. (1991). An RGD spacing of 440 nm is sufficient for integrin alpha V beta 3-mediated fibroblast spreading and 140 nm for focal contact and stress fiber formation. *J. Cell Biol.* **114,** 1089–1100.

Meller, D., Peters, K., and Meller, K. (1997). Human cornea and sclera studied by atomic force microscopy. *Cell Tissue Res.* **288,** 111–118.

Miyamoto, S., Akiyama, S. K., and Yamada, K. M. (1995). Synergistic roles for receptor occupancy and aggregation in integrin transmembrane function. *Science* **267,** 883–885.

Mrksich, M., and Whitesides, G. M. (1997). Using self-assembled monolayers that present oligo (ethylene glycol) groups to control the interactions of proteins with surfaces. *ACS Symp. Ser.* **680,** 361–373.

Pfaff, M., Tangemann, K., Muller, B., Gurrath, M., Muller, G., Kessler, H., Timpl, R., and Engel, J. (1994). Selective recognition of cyclic RGD peptides of NMR defined conformation by alpha IIb beta 3, alpha V beta 3 and alpha 5 beta 1 Integrins. *J. Biol. Chem.* **269,** 20233–20238.

Ploetz, C., Zycband, E. I., and Birk, D. E. (1991). Collagen fibril assembly and deposition in the developing dermis—segmental deposition in extracellular compartments. *J. Struct. Biol.* **106,** 73–81.

Pompe, T., Renner, L., and Werner, C. (2005). Nanoscale features of fibronectin fibrillogenesis depend on protein-substrate interaction and cytoskeleton structure. *Biophys. J.* **88**(1), 527–534.

Roberts, C., Chen, C. S., Mrksich, M., Martichonok, V., Ingber, D. E., and Whitesides, G. M. (1998). Using mixed self-assembled monolayers presenting RGD and (EG)(3)OH groups to characterize long-term attachment of bovine capillary endothelial cells to surfaces. *J. Am. Chem. Soc.* **120,** 6548–6555.

Ruoslahti, E., and Obrink, B. (1996). Common principles in cell adhesion. *Exp. Cell Res.* **227,** 1–11.

Sniadecki, N. J., Desai, R. A., Ruiz, S. A., and Chen, C. S. (2006). Nanotechnology for cell-substrate interactions. *Ann. Biomed. Eng.* **34**(1), 59–74.

Spatz, J. P., Mößmer, S., and Möller, M. (1996a). Mineralization of gold nanoparticles in a block copolymer microemulsion. *Chem. Eur. J.* **2,** 1552–1555.

Spatz, J. P., Roescher, A., and Möller, M. (1996b). Gold Nanoparticles in micellar Poly(styrene)-b-Poly(ethylene oxide) films–size and interparticle distance control in monoparticulate films. *Adv. Mater.* **8,** 337–340.

Spatz, J. P., Sheiko, S., and Möller, M. (1996c). Ion-stabilized block copolymer micelles: Film formation and intermicellar interaction. *Macromolecules* **29,** 3220–3226.

Spatz, J. P., Mößmer, S.,Hartmann, C., Möller, M., Herzog, T., Krieger, M., Boyen, H.-G., and Ziemann, P. (2000). Ordered deposition of inorganic clusters from micellar block copolymer films. *Langmuir* **16,** 407–415.

Vogel, V., and Sheetz, M. (2006). Local force and geometry sensing regulate cell functions. *Nat. Rev.* **7,** 265–275.

Wang, R. L. C., Kreuzer, H. J., and Grunze, M. (1997). Molecular conformation and solvation of oligo (ethylene glycol)-terminated self-assembled monolayers and their resistance to protein adsorption. *J. Phys. Chem.* **B101,** 9767–9773.

Xiong, J. P., Stehle, T., Zhang, R., Joachimiak, A., Frech, M., Goodman, S. L., and Arnaout, M. A. (2002). Crystal structure of the extracellular segment of integrin αVβ3 in complex with an Arg-Gly-Asp ligand. *Science* **296,** 151–155.

Zamir, E., and Geiger, B. (2001a). Molecular complexity and dynamics of cell-matrix adhesions. *J. Cell Sci.* **114,** 3583–3590.

Zamir, E., and Geiger, B. (2001b). Components of cell-matrix adhesions. *J. Cell Sci.* **114,** 3577–3579.